energies

MDPI

Article

Active Distribution Network Expansion Planning Based on Wasserstein Distance and Dual Relaxation

Jianchu Liu [1], Xinghang Weng [2], Mingyang Bao [3], Shaohan Lu [3,*] and Changhao He [1]

[1] Zhongshan Power Supply Bureau, Guangdong Power Grid Co., Ltd., Zhongshan 528405, China; thefondo@163.com (J.L.); 13791336806@163.com (C.H.)
[2] Power Grid Planning Center of Guangdong Power Grid Co., Ltd., Guangzhou 510308, China; patrick1999@foxmail.com
[3] The School of Electrical and Information Engineering, Tianjin University, Tianjin 300072, China; 3019234394@tju.edu.cn
* Correspondence: shaohan_lu@tju.edu.cn

Abstract: In the future, a high proportion of distributed generations (DG) will be integrated into the distribution network. The existing active distribution network (ADN) planning methods have not fully considered multiple uncertainties, differentiated regulation modes or the cost of multiple types of interconnection switches. Meanwhile, it is difficult to solve large-scale problems at small granularity. Therefore, an expansion planning method of ADN considering the selection of multiple types of interconnection switches is proposed. Firstly, a probability distribution ambiguity set of DG output and electrical-load consumption based on the Wasserstein distance is established for dealing with the issue of source-load uncertainty. Secondly, a distributionally robust optimization model for collaborative planning of distribution network lines and multiple types of switches based on the previously mentioned ambiguity set is established. Then, the original model is transformed into a mixed integer second-order cone programming (SOCP) model by using the convex relaxation method, the Lagrangian duality method and the McCormick relaxation method. Finally, the effectiveness of the proposed method is systematically verified using the example of Portugal 54. The results indicate that the proposed method raises the annual net profit by nearly 5% compared with the traditional planning scheme and improves the reliability and low-carbon nature of the planning scheme.

Keywords: expansion planning; soft open point (SOP); interconnection switches; distributionally robust optimization; active distribution network

Citation: Liu, J.; Weng, X.; Bao, M.; Lu, S.; He, C. Active Distribution Network Expansion Planning Based on Wasserstein Distance and Dual Relaxation. *Energies* **2024**, *17*, 3005. https://doi.org/10.3390/en17123005

Academic Editor: Hugo Morais

Received: 31 May 2024
Revised: 12 June 2024
Accepted: 16 June 2024
Published: 18 June 2024

1. Introduction

As the global greenhouse effect continues to intensify, it has become the consensus of all countries around the world to comprehensively promote carbon emission reduction under the guidance of the United Nations Framework Convention on Climate Change (UNFCCC). As an important form of energy terminal, the cleaner transformation of the power domain will be directly related to the effect of global carbon emission reduction. Under this background, the large-scale promotion of the construction of distributed generations (DG) has become an important path for the cleaner transformation of power systems. However, the volatility, intermittency and uncontrollability of DG bring great challenges to the safe operation of power systems, which may cause a series of problems such as overvoltage and line overload in the distribution network when a large number of DGs are integrated into the distribution network [1,2]. The continuous power regulation ability of soft open points (SOP) and the network reconfiguration based on sectional and interconnected switches can fully consider the source-load timing matching between different feeders to change the overall power flow, thus improving renewable energy accommodation, equipment utilization and the safety of the distribution system [3]. Therefore, it is significant to study

the collaborative planning of distribution lines, SOPs and interconnection switches, while considering the economic cost and DG accommodation.

As a means of differentiated regulation in ADN, considering the collaborative planning of SOPs and interconnection switches in the expansion planning can reduce the construction demand of power equipment, and enhance the economics of the planning scheme. Ref. [4] established a mathematical model for optimal configuration of interconnection switches for distribution lines containing PV. Compared with the interconnection switch, a SOP has more flexible power flow regulation capability, which is significant for enhancing the accommodation of renewable energy and achieving Chinese "dual-carbon goal". On this basis, Refs. [5,6] studied the collaborative planning method of SOPs and DGs and proposed a bi-level coordinated programming model. Ref. [7] proposed an ADN expansion planning method with SOPs accessed, which can cooperatively plan the location and capacity of devices such as lines, SOPs, and energy storage systems (ESS). SOP, as flexible switch, has a stronger regulation ability than the step regulation of an interconnection switch. However, most SOPs are based on power electronic equipment such as back-to-back converters, which have relatively high construction costs [8,9]. If only important locations are installed with SOPs, and interconnection switches are still installed in other locations, it can ensure the optimized operation of the system and reduce planning costs. So, the collaborative planning of SOPs and interconnection switches is more in line with the actual construction demands. Ref. [10] proposed a collaborative planning model for SOPs and interconnection switches based on a stochastic scenario to simultaneously determine the collaborative planning scheme and optimal operating strategy of SOPs and interconnection switches, but the paper did not consider line expansion planning. After referring to the literature, there is currently scarce literature on the collaborative planning of distribution network lines and multiple types of switches. Most of the literature only studied the collaborative planning of SOPs and lines, or SOPs and interconnection switches, and considers the deployment of lines or interconnection switches as the research boundary. The impact of collaborative planning and regulation of SOPs and interconnection switches on expansion planning need to be studied in the future.

In addition, the DG and load uncertainty is an important factor affecting the economy and security of the expansion planning scheme, and the different ways of dealing with the uncertainty will affect the evaluation of the net-load and then affect the location and capacity of equipment [11]. Currently, stochastic optimization, interval optimization, robust optimization, and distributionally robust optimization are commonly used in the study of uncertainty. Among them, stochastic optimization relies on the probability distribution of historical data [12,13], interval optimization is limited by the problem size [14,15], and the plans resulting from using robust optimization are often too conservative [16], while distributionally robust optimization can overcome the above shortcomings. The temporal probability distribution curves can be obtained through a large amount of historical data, but these are based on limited data statistics and there is still a gap between these curves and the actual data. By using the distributionally robust optimization method, the optimal scheduling under the worst scenario can be obtained within the allowable error range. On one hand, it can obtain the temporal characteristics of the source and load like stochastic optimization. On the other hand, it can also improve the robustness of the planning scheme and enhance the reliability of the scheme under bad conditions. Refs. [17,18] both established the distributionally robust optimization operation model for integrated energy systems, and analyzed and verified the advantage of distributionally robust optimization.

The distributionally robust optimization model has various types of ambiguity sets, such as an ambiguity set based on generalized moment information and an ambiguity set based on statistical distance [19,20]. Among them, the ambiguity set based on the Wasserstein distance is more popular, and its probability distribution is contained in the Wasserstein sphere with a certain confidence level [21]. Ref. [22] proposed a scenario-based stochastic modeling approach based on the Wasserstein distance and K-medoids to deal with the stochasticity of DG, and then built and solved a multi-objective collaborative

planning model for ADN. Ref. [23] used a multi-scenario approach based on the Wasserstein distance to deal with DG uncertainty and proposed an AC/DC optimized extended planning model for distribution networks from the perspective of the distribution system operator (DSO). Ref. [24] used the optimal scenario generation technique based on the Wasserstein distance to deal with the uncertainty of WT and PV and proposed an AND planning method considering SOPs and the operating characteristics of DGs. However, Refs. [22–24] only utilized the ability of the Wasserstein distance to measure probability distribution differences and generated discretized scenes using the Wasserstein distance. But these references did not introduce the Wasserstein distance into the ambiguity set of the distributionally robust optimization model. Ref. [25] established a Wasserstein ambiguity set for each uncertain factor in the carbon-oriented economic dispatch for day-ahead market and proposed a carbon-oriented Wasserstein distributionally robust scheduling model. It can be seen from the above references that distributionally robust optimization based on the Wasserstein distance has certain advantages in dealing with the DG and load uncertainty. Currently, research on ADN planning rarely use the distributionally robust optimization model based on the Wasserstein distance to deal with source-load uncertainty. If this method is applied to the multi-type interconnection switches and lines expansion planning problem, it will better balance the economy and robustness of the scheme. However, after considering the large-scale network reconfiguration requirements, the distributionally robust model based on the Wasserstein distance will contain many nonlinear terms, and further research is needed to deal with the nonlinear terms in model relaxation that can guarantee the optimality and computational efficiency.

In summary, to solve the above problems, this paper proposes a cooperative expansion planning method for distribution lines, SOPs and interconnection switches based on the Wasserstein distance and dual relaxation. Firstly, in order to overcome the difficulty of accurately obtaining the probability distribution of uncertainty in the power distribution system, this paper establishes a probability distribution ambiguity set of DG and load based on the Wasserstein distance and a min–max distributionally robust optimization model for the collaborative planning of distribution lines and multi-type interconnection switches. Secondly, in order to solve the problem caused by the model's nonlinearities, the model is transformed by the convex relaxation, duality method, and McCormick relaxation. Finally, the effectiveness of the proposed method is systematically verified with the Portugal 54 nodes system, which improves the annual net profits by nearly 5% compared with the traditional planning scheme and ensures the security and low-carbon nature of the distribution network construction scheme, while the proposed relaxation method is able to balance the relaxation margins with the solution speed.

2. Theoretical Basis

2.1. Principle and Physical Model of SOP and Interconnection Switch

An interconnection switch is connected between two radiating feeders and can achieve load transfer between the two feeders. The main access mode of the SOP in the distribution network is closed-loop connection between feeders to replace the normal open circuit point or interconnection switch in the ADN. This paper considers the installation of a two-port SOP and an interconnection switch between radiating feeders, as shown in Figure 1.

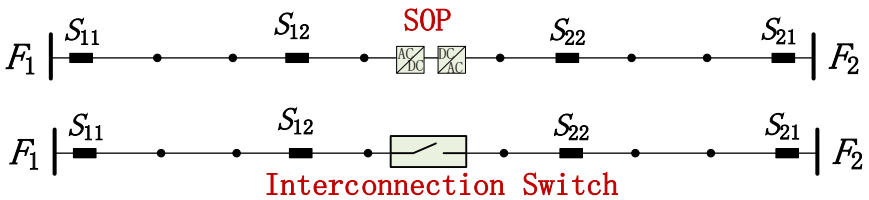

Figure 1. Access mode of SOP and interconnection switch.

In Figure 1, F_1 and F_2 are two radiating feeders, and S_{11}, S_{12}, S_{21}, and S_{22} are the sectionalizing switches used for network reconfiguration in the two feeders. Control of the SOP is achieved by full-controlled power electronic devices, and back-to-back voltage source converters are commonly used. The controllable variables of the SOP include the active power and reactive power output from the port, while the interconnection switch can only control the on–off state of the circuit. Compared with interconnection switches, SOPs can accurately control power flow at lower operating costs, avoiding the risks caused by frequent switch operations, and greatly improving the flexibility and speed of ADN control.

2.2. The Probability Distribution Ambiguity Set Based on Wasserstein Distance

The actual timing characteristics of probability distribution of DGs and loads are often difficult to obtain directly from the real world. Optimization methods based on probability distribution will have strong uncertainties. In order to reasonably deal with the DG and load uncertainty, the distributionally robust optimization method assumes that the distribution function is not explicit but is in an ambiguity set. The ambiguity set is constructed by the incomplete distribution information of random variables, and it is also necessary to ensure that the distributionally robust optimization model of the realistic problem scale can be solved within the allowed time range. There are two main types of distributionally robust optimization ambiguity sets, including ambiguity sets based on generalized moment information and those based on statistical distance. The ambiguity set based on the Wasserstein distance belongs to the second category. The Wasserstein distance is used to describe the distance between the true distribution and the reference distribution, which is suitable for the treatment of source-load uncertainty. Based on the above analysis, this paper establishes a probability distribution ambiguity set of source and load timing characteristics based on the Wasserstein distance for dealing with uncertainty.

Define the random variables sets as $\overset{\wedge}{\xi}^{dg}$ and $\overset{\wedge}{\xi}^{load}$, respectively, as the historical observations sets as $\left\{\overset{\wedge}{\xi}_1^{dg}, \overset{\wedge}{\xi}_2^{dg}, \cdots, \overset{\wedge}{\xi}_L^{dg}\right\}$ and $\left\{\overset{\wedge}{\xi}_1^{load}, \overset{\wedge}{\xi}_2^{load}, \cdots, \overset{\wedge}{\xi}_L^{load}\right\}$ for DG and load, where L is the sample size. Notably, this modeling method is applicable to various types of DGs, and the number of ambiguity sets is equal to the number of DG types. Due to the different generation patterns of various types of DGs, the parameters and reference distributions in the model are different, and thus the final ambiguity sets are also different. This article mainly considers wind turbines and photovoltaics. We use the Dirac function to construct the reference distributions $\hat{P}_{REF}^{dg}$ and $\hat{P}_{REF}^{load}$ for $\overset{\wedge}{\xi}^{dg}$ and $\overset{\wedge}{\xi load}$ [26]:

$$\begin{aligned} \hat{P}_{REF}^{dg} &= \frac{1}{L}\sum_{l=1}^{L}\delta_{\hat{\xi}_l}^{dg} \\ \hat{P}_{REF}^{load} &= \frac{1}{L}\sum_{l=1}^{L}\delta_{\hat{\xi}_l}^{load} \end{aligned} \tag{1}$$

where $\delta_{\hat{\xi}_l}^{dg}$ and $\delta_{\hat{\xi}_l}^{load}$ are the Dirac functions of $\hat{\xi}_{l,t}^{dg}$ and $\hat{\xi}_{l,t}^{load}$; $\hat{\xi}_{l,t}^{dg}$ and $\hat{\xi}_{l,t}^{load}$ are the energy coefficients of DGs and loads at time t with sample l as the reference, which are historical observation data.

The reference distribution can be viewed as an estimation of the true distribution. In order to represent the gap between the true distribution and the reference distribution, introduce the Wasserstein distance as follows:

$$\begin{aligned} d_{\mathrm{w1}}(P_{dg}^{*}, \hat{P}_{REF}^{dg}) &= \inf\left\{\int_{\Omega^2}\left\|\xi^{dg} - \overset{\wedge}{\xi}^{dg}\right\|\Pi(\mathrm{d}\xi^{dg}, \mathrm{d}\overset{\wedge}{\xi}^{dg})\right\} \\ d_{\mathrm{w2}}(P_{load}^{*}, \hat{P}_{REF}^{load}) &= \inf\left\{\int_{\Omega^2}\left\|\xi^{load} - \overset{\wedge}{\xi}^{load}\right\|\Pi(\mathrm{d}\xi^{load}, \mathrm{d}\overset{\wedge}{\xi}^{load})\right\} \end{aligned} \tag{2}$$

where $d_w(\cdot)$ denotes the Wasserstein distance; ξ^{dg} and ξ^{load} are the random variables sets obeying the true distributions P^*_{dg} and P^*_{load}; $\Pi(\mathrm{d}\xi^{dg}, \mathrm{d}\hat{\xi}^{dg})$ denotes the joint probability distribution of $\mathrm{d}\xi^{dg}$ and $\mathrm{d}\hat{\xi}^{dg}$, and $\Pi(\mathrm{d}\xi^{load}, \mathrm{d}\hat{\xi}^{load})$ is the same; $\|\bullet\|$ denotes the first-order norm; $\mathrm{d}\xi^{dg}$ and $\mathrm{d}\xi^{load}$ are the differentials of ξ^{dg} and ξ^{load}; Ω^2 denotes the support space of the random variables; $\inf\{\bullet\}$ denotes the infimum function.

Based on the above, construct the Wasserstein sphere centered on the reference distribution $\hat{P}^{dg}_{REF}$ and $\hat{P}^{load}_{REF}$ with radius as ε_{dg} and ε_{load}, the equation is shown below:

$$\begin{aligned} B_{\varepsilon_{dg}}\left(\hat{P}^{dg}_{REF}\right) &= \left\{P^*_{dg} \in \Gamma_{dg} \middle| d_{\mathrm{W}}(P^*_{dg}, \hat{P}^{dg}_{REF}) \leqslant \varepsilon_{dg}\right\} \\ B_{\varepsilon_{load}}\left(\hat{P}^{load}_{REF}\right) &= \left\{P^*_{load} \in \Gamma_{load} \middle| d_{\mathrm{W}}(P^*_{load}, \hat{P}^{load}_{REF}) \leqslant \varepsilon_{load}\right\} \end{aligned} \tag{3}$$

Among them, Γ_{dg} is the space of all values supporting P^*_{dg} and Γ_{load} is the same. Equation (3) indicates that the Wasserstein distance between the true and reference distribution of DG and load is no more than the sphere radius.

Relevant references prove that the radius ε_{dg} and ε_{load} of the Wasserstein sphere is a function of the sample size L and the confidence level α^{dg}. Confidence level is a concept used to indicate the level of confidence in parameter estimates. The confidence level is usually a number between 0 and 1. When the confidence level is set to 0, distributionally robust optimization degenerates into stochastic optimization, and when set to 1, it degenerates into robust optimization. By adjusting the confidence level, the robustness of the distributionally robust optimization can be adjusted to balance economy and robustness. The relevant equations are as follows:

$$\begin{aligned} P(d_{\mathrm{w}}(P^*_{dg}, \hat{P}^{dg}_{REF}) \leqslant \varepsilon^{\mathrm{dg}}) &= 1 - \exp(-\tfrac{(\varepsilon^{\mathrm{dg}})^2}{2S^2}L) \\ P(d_{\mathrm{w}}(P^*_{load}, \hat{P}^{load}_{REF}) \leqslant \varepsilon^{load}) &= 1 - \exp(-\tfrac{(\varepsilon^{load})^2}{2S^2}L) \\ \varepsilon^{dg}(L, \alpha^{dg}) &= S\sqrt{\tfrac{2}{L}\ln(\tfrac{1}{1-\alpha^{dg}})} \\ \varepsilon^{load}(L, \alpha^{load}) &= S\sqrt{\tfrac{2}{L}\ln(\tfrac{1}{1-\alpha^{load}})} \end{aligned} \tag{4}$$

where P ($\bullet$) is the spherical probability function; S defines the maximum Wasserstein distance between any two elements in Ω^2, calculated as follows:

$$S = \min_{\mu \geqslant 0} 2\sqrt{\frac{1}{2\mu}\left(1 + \ln\left(\frac{1}{L}\sum_{l=1}^{L}\exp(\mu\|\hat{\xi}_l - \hat{\kappa}\|)\right)\right)} \tag{5}$$

Among them, $\hat{\kappa}$ is the mean value of samples, and μ is a variable greater than 0.

3. Distributionally Robust Collaborative Planning Model Based on Wasserstein Distance

Considering the effect of the source-load uncertainty in planning and operation is beneficial to improve the practical value of planning and operation results. Therefore, this section combines the ambiguity set of probability distribution based on the Wasserstein distance established in the previous section to establish a distributionally robust collaborative planning model based on the Wasserstein distance. In this model, the planning variables include the planning location and capacity of SOPs, the location of interconnection switches, and the situation of the expansion lines. Additionally, the operational variables include the power flow situation, the operation status of devices which include the ESS, SOPs, and interconnection switches, the response power of demand response (DR), the reduction power of DG and the uncertainty variables of the Wasserstein distance.

3.1. Objective Function

After considering the source-load uncertainty, the objective function is of the min-max type, which means to find the solution with the best economics under the worst scenario. The objective function is to minimize the annual net cost during the planning period, including the investment cost C^{inv} and the operation cost C^{ope}. The investment cost includes the equivalent annual construction cost of SOPs, interconnection switches, and lines. The operation cost includes the SOPs operation and maintenance cost C^{om}_{sop}, the interconnection switches action cost C^{om}_{switch}, the ESS operation and maintenance cost C^{om}_{ess}, the demand response cost C_{DR}, and the penalty cost for wind and solar power discard C_{DG}, the power loss cost C_{loss}, the purchase and sale net cost $C_{buy} - C_{sell}$. The calculation equation is shown below:

$$\min_{Y} \max_{B} C = C^{inv} + C^{ope} \tag{6}$$

$$C^{inv} = C^{inv}_{sop} + C^{inv}_{switch} + C^{inv}_{line} \tag{7}$$

$$C^{ope} = C^{om}_{sop} + C^{om}_{switch} + C^{om}_{ess} + C_{DR} + C_{loss} + C_{buy} - C_{sell} \tag{8}$$

Among them, Y denotes the set composed of deterministic variables during the planning and operation process, such as the planning location and capacity of SOPs and the planning location of interconnection switches; $B = \left\{ \Delta\xi^{load}_{l,t}, \Delta\xi^{dg}_{l,t} \right\}$ is the set composed of the deviation between the true distribution and the reference distribution of the source-load timing characteristics, which is uncertainty variable. The equation for each cost is shown below:

$$C^{inv}_{sop} = \tau^{sop} \sum_{ij \in \Psi_{sop}} c_{sop} S^{sop}_{ij} \tag{9}$$

$$C^{inv}_{switch} = \tau^{switch} \sum_{ij \in \Psi_{switch}} c_{switch} Y^{switch}_{ij} \tag{10}$$

$$C^{inv}_{line} = \tau^{line} \sum_{L_{ij} \in \Psi_{line}} c_{line} Y^{line}_{ij} L_{ij} \tag{11}$$

$$\tau^{x} = \frac{r(1+r)^{b^x}}{(1+r)^{b^x} - 1} \tag{12}$$

$$C^{om}_{sop} = \lambda_{sop} \sum_{ij \in \Psi_{sop}} c_{sop} S^{sop}_{ij} \tag{13}$$

$$C^{om}_{switch} = \lambda_{switch} \sum_{ij \in \Psi_{switch}} c_{switch} \left(\sum_{t=1}^{T} \left| \alpha^{switch}_{ij,t} - \alpha^{switch}_{ij,t-1} \right| \right) \tag{14}$$

$$C^{om}_{ess} = \sum_{i \in \Psi_{ess}} \sum_{t=1}^{T} c^{P}_{ess} \left(\eta^{essch}_{p} P^{essch}_{i,t} - P^{essdch}_{i,t} / \eta^{essdch}_{p} \right) \tag{15}$$

$$C_{DR} = \sum_{i \in \Psi_{load}} \sum_{t=1}^{T} c_{DR} \Delta P^{DR}_{i,t} \tag{16}$$

$$C_{DG} = \sum_{i \in \Psi_{dg}} \sum_{t=1}^{T} c_{DG} P^{dgcut}_{i,t} \tag{17}$$

$$C_{loss} = c_{loss} \left(\sum_{ij \in \Psi_{b}} \sum_{t=1}^{T} I^{2}_{ij,t} r_{ij} + \sum_{i \in \Psi_{sop}} \sum_{t=1}^{T} P^{SOP,L}_{i,t} \right) \tag{18}$$

In this case, the cost of purchasing electricity from the higher grid C_{buy} and the revenue from electricity sales C_{sell} contain uncertainty variables, as shown in the following equations:

$$C_{buy} = c_{buy} \sum_{\substack{i \in \Psi_{node} \\ ij \in \Psi_b}} \sum_{t=1}^{T} \left(\overset{\sim}{P_{i,t}^{load}} + I_{ij,t}^2 r_{ij} + \sum_{t=1}^{T} P_{i,t}^{SOP,L} - \Delta P_{i,t}^{DR} - \overset{\sim}{P_{i,t}^{dg}} + P_{i,t}^{dgcut} + P_{i,t}^{essch} - P_{i,t}^{essdch} \right) \tag{19}$$

$$C_{sell} = c_{sell} \sum_{\substack{i \in \Psi_{node} \\ ij \in \Psi_b}} \sum_{t=1}^{T} \left(\overset{\sim}{P_{i,t}^{load}} - \Delta P_{i,t}^{DR} - \overset{\sim}{P_{i,t}^{dg}} + P_{i,t}^{dgcut} - P_{i,t}^{essdch} + P_{i,t}^{essch} \right) \tag{20}$$

where $\overset{\sim}{P_{i,t}^{load}}$ and $\overset{\sim}{P_{i,t}^{dg}}$ are the actual value of load electric use and DG output in node i for time t. τ^x denotes the equal annual value coefficient of equipment x; r is the discount rate; b is the service life of the equipment; and x is the type of equipment, including SOPs, interconnection switches, and lines; c_{SOP} denotes the SOP construction cost of per capacity unit; c_{switch} denote the per-unit construction cost of interconnection switch; c_{line} denotes the line construction cost per length unit; c_{ess}^P denotes the operating cost per power unit; c_{DR} denotes the unit price of DR incentives; c_{DG} denotes the unit penalty price of abandoning wind and electricity; c_{buy} and c_{sell} represent the unit price for purchasing power from the higher-level grid and for selling power to customers; Ψ_{SOP}, Ψ_{Switch} and Ψ_{line} represent the candidate sets of SOPs, interconnection switches and lines construction locations; Ψ_{ess}, Ψ_{load}, Ψ_b and Ψ_{node} represent the set of the ESS and loads locations, the set of branches, and the set of nodes; S_{ij}^{sop} represents the capacity of an SOP between the node i and j; Y_{ij}^{switch} is a 0–1 variable, and 1 indicates that a new interconnection switch is built between the node i and j; Y_{ij}^{line} is a 0–1 variable, and 1 indicates that a line between the node i and j, the length of the expansion line is L_{ij}; λ_{sop} and λ_{switch} are the annual operation and maintenance cost coefficients for SOPs and interconnection switches; $\alpha_{ij,t}^{switch}$ is the on/off state of the interconnection switch between the node i and j for time t, where 0 represents open and 1 represents closed; E_i^{ess}, $P_{i,t}^{essch}$ and $P_{i,t}^{essdch}$, respectively, represent the ESS capacity, charging and discharging power of node i connected fot time t; η_p^{essch}, η_p^{essdch} are efficiency coefficients for energy storage charging and discharging; $\Delta P_{i,t}^{DR}$ is the demand response reduction in the load accessed to node i at time t; $I_{ij,t}^2$ and r_{ij} denote the current square and resistance of branch ij at time t; $P_{i,t}^{SOP,L}$ denotes the loss power of the SOP port connected to node i at time t; $P_{i,t}^{dgcut}$ denotes the reduction in DG connected to node i at time t.

3.2. Constraints

3.2.1. Planning Constraints

(1) New line state:

$$Y_{ij}^{line} \in \{0,1\}, \forall ij \in \Psi_{line} \tag{21}$$

This equation constrains the 0–1 variable Y_{ij}^{line}, 1 means that the line between node i and j is subjected to be expansion planning, and 0 means not; Ψ_{line} is the set of line expansion candidate locations.

(2) SOP installation location and capacity:

$$\begin{cases} 0 \le m_{ij}^{sop} \le m_{\max}^{sop} \\ S_{ij}^{sop} = m_{ij}^{sop} S_{rated}^{sop} \end{cases}, \forall ij \in \Psi_{sop} \tag{22}$$

where m_{ij}^{sop} is a non-negative integer variable indicating the number of SOP units installed between node i and j; $m_{\max}^{sop}$ is the maximum number of units installed; S_{rated}^{sop} is the SOP unit capacity, and SOP capacity S_{ij}^{sop} is m_{ij}^{sop} times the SOP unit capacity.

(3) Interconnection switch installation location:

$$Y_{ij}^{switch} \in \{0,1\}, ij \in \Psi_{switch} \tag{23}$$

The above equation constrains the 0–1 variable Y_{ij}^{switch}, 1 means that a switch will be built between node i and j, and 0 means not, and the set of candidate locations for interconnection switch is Ψ_{switch}.

(4) Network topology constraints:

$$Y_{ij}^{line} + Y_{ij}^{switch} + Y_{ij}^{sop} \leq 1, \forall i, j \in \Psi_{node}, i \neq j \tag{24}$$

$$\beta_{ij,t} + \beta_{ji,t} = \alpha_{ij,t}^{line} + \alpha_{ij,t}^{switch}, \forall i, j \in \Psi_{node}, i \neq j \tag{25}$$

$$\begin{gathered} \sum_{j \in \Psi_{load}} \beta_{ij,t} = 1 \\ \sum_{j \in \Psi_{sta}} \beta_{ij,t} = 0 \end{gathered} \tag{26}$$

$$\begin{gathered} 0 \leq \alpha_{ij,t}^{line} \leq Y_{ij}^{line} \\ 0 \leq \alpha_{ij,t}^{switch} \leq Y_{ij}^{switch} \end{gathered} \tag{27}$$

Equation (24) means that the lines, interconnection switches and SOPs should not be duplicated in construction. Equations (25) and (26) mean that the substation has no parent node and the rest nodes have only one parent node, Ψ_{sta} is the set of substation nodes. β_{ij} is a binary variable indicating whether node i is the parent node of node j, and it takes 1 when node i is the parent node of node j, otherwise it takes 0; $\alpha_{ij,t}^{line}$ and $\alpha_{ij,t}^{switch}$ indicate the on/off status of the branch ij at time t, and it equals to 1 indicating the connection, and it equals to 0 indicating the disconnection.

3.2.2. Operational Constraints

(1) Power flow and power balance constraints:

$$\begin{gathered} \sum_{j \in \kappa(i)} P_{ij,t} - \sum_{k \in \rho(i)} \left(P_{ki,t} - r_{ki} I'_{ki,t} \right) = P_{i,t}^{\text{in}}, \forall i \in \Psi_{\text{N}} \\ \sum_{j \in \kappa(i)} Q_{ij,t} - \sum_{k \in \rho(i)} \left(Q_{ki,t} - x_{ki} I'_{ki,t} \right) = Q_{i,t}^{\text{in}}, \forall i \in \Psi_{\text{N}} \end{gathered} \tag{28}$$

$$\begin{gathered} P_{i,t}^{in} = P_{i,t}^{sta} + \overset{\sim}{P_{i,t}^{dg}} - P_{i,t}^{sop} - P_{i,t}^{essch} + P_{i,t}^{essdch} - \overset{\sim}{P_{i,t}^{load}} + \Delta P_{i,t}^{DR} - P_{i,t}^{dgcut} \\ Q_{i,t}^{in} = Q_{i,t}^{sta} - Q_{i,t}^{sop} - Q_{i,t}^{load} \end{gathered} \tag{29}$$

$$I'_{ij,t} V_{i,t} - P_{ij,t}^2 - Q_{ij,t}^2 = 0, \forall ij \in \Psi_{line} \tag{30}$$

where $P_{ij,t}$ and $Q_{ij,t}$ are the active and reactive power on branch ij at time t; $I'_{ki,t}$ is the square of the current of branch ki at time t; $V_{i,t}$ is the square of the voltage of node i at time t; $P_{i,t}^{\text{in}}$ and $Q_{i,t}^{\text{in}}$ are the injected active and reactive power at node i at time t; $\kappa(i)$ and $\rho(i)$ denote the set of child nodes and the set of parent nodes of node i; $P_{i,t}^{sta}$ and $Q_{i,t}^{sta}$ are the injected active and reactive power of the substation. Constraint (29) contains uncertainty variables.

(2) Voltage-drop constraints considering network reconfiguration:

$$\begin{gathered} V_{i,t} - V_{j,t} \geq 2(r_{ij} P_{ij,t} + x_{ij} Q_{ij,t}) - (r_{ij}^2 + x_{ij}^2) I_{ij,t}^2 - M(1 - \alpha_{ij,t}^{line}), \forall ij \in \Psi_{line} \\ V_{i,u,t} - V_{j,u,t} \leq 2(r_{ij} P_{ij,t} + x_{ij} Q_{ij,t}) - (r_{ij}^2 + x_{ij}^2) I_{ij,t}^2 + M\left(1 - \alpha_{ij,t}^{line}\right), \forall ij \in \Psi_{line} \end{gathered} \tag{31}$$

where M is a very large number, indicating that if network reconfiguration results in the disconnection of original lines, the voltage drop between the two nodes can take any arbitrary value, otherwise it must satisfy conventional constraints; r_{ij} and x_{ij} are the resistance and reactance of the branch ij.

(3) Voltage security and branch current constraint:

$$V_{\min,i}^2 \le V_{i,t} \le V_{\max,i}^2, i \in \Psi_{node} \tag{32}$$

$$0 \le I'_{ij,t} \le \left(\alpha_{ij,t}^{line} + \alpha_{ij,t}^{switch}\right) I_{\max,ij}^2, \forall ij \in \Psi_{line} \tag{33}$$

where $V_{\min,i}^2$ and $V_{\max,i}^2$ are the minimum and maximum values of the voltage at node i; $I_{\max,ij}^2$ is the maximum value of the current at branch ij. Equation (33) shows that if the branch is connected, the current satisfies the normal constraint, otherwise the current is zero.

(4) SOP operation constraints:

$$P_{i,t}^{\mathrm{SOP}} + P_{j,t}^{\mathrm{SOP}} + P_{i,t}^{\mathrm{SOP,L}} + P_{j,t}^{\mathrm{SOP,L}} = 0 \tag{34}$$

$$\begin{cases} P_{i,t}^{\mathrm{SOP,L}} = \eta_{sop}\sqrt{\left(P_{i,t}^{\mathrm{SOP}}\right)^2 + \left(Q_{i,t}^{\mathrm{SOP}}\right)^2} \\ P_{j,t}^{\mathrm{SOP,L}} = \eta_{sop}\sqrt{\left(P_{j,t}^{\mathrm{SOP}}\right)^2 + \left(Q_{j,t}^{\mathrm{SOP}}\right)^2} \end{cases} \tag{35}$$

$$\begin{cases} \sqrt{\left(P_{i,t}^{\mathrm{SOP}}\right)^2 + \left(Q_{i,t}^{\mathrm{SOP}}\right)^2} \le S_{ij}^{\mathrm{SOP}} \\ \sqrt{\left(P_{j,t}^{\mathrm{SOP}}\right)^2 + \left(Q_{j,t}^{\mathrm{SOP}}\right)^2} \le S_{ij}^{\mathrm{SOP}} \end{cases} \tag{36}$$

In the equations, if the SOP is installed between nodes i and j, $P_{i,t}^{\mathrm{SOP}}$ and $P_{j,t}^{\mathrm{SOP}}$ represent the active power flowing into the SOP from nodes i and j at time t, and if it is negative, it represents the outflow power; $P_{i,t}^{\mathrm{SOP,L}}$ represents the power loss caused by the inflow or outflow of the SOP from node i at time t; $Q_{i,t}^{\mathrm{SOP}}$ and $Q_{j,t}^{\mathrm{SOP}}$ represent the reactive power flowing into the SOP from nodes i and j at time t, and if it is negative, it represents the outflow reactive power; η_{sop} is the loss coefficient of the SOP; S_{ij}^{SOP} represents the capacity of the SOP between nodes i and j.

(5) ESS operation constraints:

$$\begin{cases} 0 \leqslant P_{i,t}^{essch} \leqslant P_{\max}^{essch} \\ 0 \leqslant P_{i,t}^{essdch} \leqslant P_{\max}^{essdch} \end{cases} \tag{37}$$

$$E_{i,t+1}^{\mathrm{ess}} = E_{i,t}^{ess}(1 - \eta_e^{ess}) + \eta_p^{essch} P_{i,t}^{essch} - \frac{P_{i,t}^{essdch}}{\eta_p^{essdch}} \tag{38}$$

$$0.2E_{\max}^{ess} \leqslant E_{i,t}^{ess} \leqslant 0.9E_{\max}^{ess} \tag{39}$$

In the equation, $P_{\max}^{essch}$ and $P_{\max}^{essdch}$ are the ESS maximum power of charging and discharging; η_e^{ess}, η_p^{essch} and η_p^{essdch} are the battery loss coefficient, charging, and discharging efficiency coefficient of energy storage; $E_{\max}^{ess}$ is the upper limit of power storage, and the storage power at each moment cannot be more than 90% of the upper limit, and cannot be less than 20%.

(6) Network reconfiguration constraint:

$$\sum_{ij \in \Psi_{line}} \left(\alpha_{ij,t}^{line} + \alpha_{ij,t}^{switch}\right) = N_{node} - N_{sta} \tag{40}$$

where N_{node} and N_{sta} are the number of nodes and substations.

(7) Constraint of the maximum allowable number of switching operations:

$$\sum_{ij\in\Psi_{switch}}\sum_{t=1}^{T}\left|\alpha_{ij,t}^{switch}-\alpha_{ij,t-1}^{switch}\right|\le N_{\max}^{\text{switch}} \tag{41}$$

where $N_{\max}^{\text{switch}}$ is maximum allowable number of switching operations in a cycle. In order to reduce the abrasion caused by multiple reconfigurations, the number of switching operations is limited here.

(8) Wind and light abandonment constraint:

$$P_{i,t}^{dgcut}\le k_{\max}^{dg}\overset{\sim}{P_{i,t}^{dg}} \tag{42}$$

where $k_{\max}^{dg}$ is the maximum reduction ratio of DG.

(9) Demand response constraints:

$$\begin{cases}-\eta_{dr}\overset{\sim}{P_{i,t}^{load,trans}}\le\Delta P_{i,t}^{DR,trans}\le\eta_{dr}\overset{\sim}{P_{i,t}^{load,trans}}\\ \sum\limits_{i\in\Psi_{trans}}\sum\limits_{t=1}^{T}\Delta P_{i,t}^{DR,trans}=0\end{cases} \tag{43}$$

$$0\le\Delta P_{i,t}^{DR,cut}\le\eta_{dr}\overset{\sim}{P_{i,t}^{load,cut}} \tag{44}$$

$$\Delta P_{i,t}^{DR}=\Delta P_{i,t}^{DR,trans}+\Delta P_{i,t}^{DR,cut} \tag{45}$$

where $\overset{\sim}{P_{i,t}^{load,trans}}$ and $\overset{\sim}{P_{i,t}^{load,cut}}$ are the real power demand of transferable load and curtailable load at node i at time t, respectively; $\Delta P_{i,t}^{DR,trans}$ and $\Delta P_{i,t}^{DR,cut}$ are the response power of transferable load and curtailable load at node i at time t; η_{dr} is the contract signing proportion of the demand response.

3.2.3. Uncertainty Constraints

Since this model uses distributionally robust optimization based on the Wasserstein distance to deal with uncertainty, it has to satisfy the Wasserstein ambiguity set constraints as shown in Equations (1)–(5). In addition, the following constraints need to be satisfied for the actual energy output/usage of DG and load:

$$\begin{aligned}\overset{\sim}{P_{i,t}^{\text{dg}}}&=P_{i,t}^{\text{dg}}\xi_{l,t}^{dg}\\ \xi_{l,t}^{dg}&=\hat{\xi_{l,t}^{dg}}+\Delta\xi_{l,t}^{dg}\end{aligned} \tag{46}$$

$$\begin{aligned}\overset{\sim}{P_{i,t}^{load}}&=P_{i,t}^{load}\xi_{l,t}^{load}\\ \xi_{l,t}^{load}&=\hat{\xi_{l,t}^{load}}+\Delta\xi_{l,t}^{load}\end{aligned} \tag{47}$$

where $\xi_{l,t}^{dg}$ and $\xi_{l,t}^{load}$ are the actual energy output/usage coefficients of DG and load at time t with sample l as the reference, and $\hat{\xi_{l,t}^{dg}}$ and $\hat{\xi_{l,t}^{load}}$ are the referential energy output/usage coefficients of DG and load at time t with sample l as the reference.

In summary, the distributionally robust planning model based on the Wasserstein distance can be organized in the following form:

$$\begin{aligned}&\min_{Y}\max_{B}C=C^{inv}+C^{ope}\\ &s.t.\begin{cases}(1)\sim(5)\\ (21)\sim(47)\end{cases}\end{aligned} \tag{48}$$

4. Solution Method

4.1. Overall Solution Framework

Since the distributionally robust planning model established in this paper is a bi-level mixed integer nonconvex nonlinear model, it is difficult to solve it directly and effectively. Here, we propose a solution method. First, the constraints should be transformed, and the nonlinear constraints of the original model should be transformed into second-order cone constraints, and the Wasserstein constraints need to be equivalently transformed. Then, the max function in the inner layer of the objective function is transformed by Lagrange duality into the min function, and then the inner and outer layers are merged to obtain a single-layer model with a min-type objective function. Finally, the nonlinear terms in the objective function are transformed, and the original model is transformed into the MISOCP model, which can be solved by solvers. The overall solution framework is shown in Figure 2.

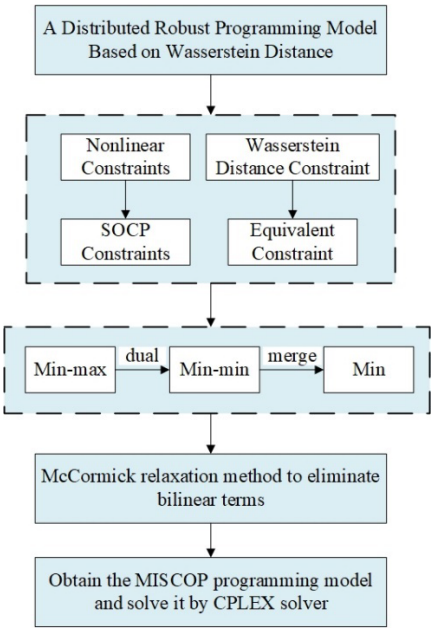

Figure 2. Flowchart of model solving.

4.2. Specific Solution Method

Next, the specific steps of the overall solution framework will be described in detail, which are mainly divided into the transformation of the constraints, the duality of the inner max-type function, and the transformation of the bilinear term of the final function.

4.2.1. Constraint Transformation

Some constraints within the distributionally robust planning model are nonlinear and must be reformulated as second-order cone constraints using the convex relaxation method to simplify computations. In addition, Wasserstein constraints also need to be transformed equivalently. The transformation equations are shown below.

The original power flow constraint (28) and the SOP operation constraint (35)–(36) are rewritten after convex relaxation [27], as shown in Equations (49)–(51):

$$\left\| \left[2P_{ij,t} 2Q_{ij,t} I'_{ij,t} - V_{i,t} \right]^{\mathrm{T}} \right\|_2 \leq I'_{ij,t} + V_{i,t} \tag{49}$$

$$\begin{cases} \left\| \left[P_{i,t}^{\mathrm{SOP}} Q_{i,t}^{\mathrm{SOP}} \right]^{\mathrm{T}} \right\|_2 \le 2 \frac{P_{i,t}^{\mathrm{SOP,L}}}{\sqrt{2}\eta_{sop}} \frac{P_{i,t}^{\mathrm{SOP,L}}}{\sqrt{2}\eta_{sop}} \\ \left\| \left[P_{j,t}^{\mathrm{SOP}} Q_{j,t}^{\mathrm{SOP}} \right]^{\mathrm{T}} \right\|_2 \le 2 \frac{P_{j,t}^{\mathrm{SOP,L}}}{\sqrt{2}\eta_{sop}} \frac{P_{j,t}^{\mathrm{SOP,L}}}{\sqrt{2}\eta_{sop}} \end{cases} \tag{50}$$

$$\begin{cases} \left\| \left[P_{i,t}^{\mathrm{SOP}} Q_{i,t}^{\mathrm{SOP}} \right]^{\mathrm{T}} \right\|_2 \le 2 \frac{S_{ij}^{\mathrm{SOP}}}{\sqrt{2}} \frac{S_{ij}^{\mathrm{SOP}}}{\sqrt{2}} \\ \left\| \left[P_{j,t}^{\mathrm{SOP}} Q_{j,t}^{\mathrm{SOP}} \right]^{\mathrm{T}} \right\|_2 \le 2 \frac{S_{ij}^{\mathrm{SOP}}}{\sqrt{2}} \frac{S_{ij}^{\mathrm{SOP}}}{\sqrt{2}} \end{cases} \tag{51}$$

If the objective function is monotonically increasing with respect to the slack viables, the SOCP relaxation is accurate, which has been proved. In addition to that, the computational complexity is relatively small in the radiation distribution network [28]. If the slack gap is small enough, we consider that SOCP relaxation meets the accuracy requirements.

The equivalent transformation of Wasserstein constraints (1)–(5) are as follows [29]:

$$\begin{aligned} &\frac{1}{L} \sum_{l \in L} \left| \Delta \xi_{l,t}^{dg} \right| \le \varepsilon_{dg} \forall t \\ &\frac{1}{L} \sum_{l \in L} \left| \Delta \xi_{l,t}^{load} \right| \le \varepsilon_{load} \forall t \end{aligned} \tag{52}$$

4.2.2. Duality of Inner Function

Due to the uncertain variables in objective function and constraints, the model needs to be organized into the following form before duality:

$$\max_{\Delta \xi} F^T x$$
$$\text{s.t.} \begin{cases} J_1 x + (\overset{\wedge}{\xi}_{l,t} + \Delta \xi_{l,t}) J_2 x = J_3 & \forall t, \forall l, \pi_{l,t} \\ G_1 x + (\overset{\wedge}{\xi}_{l,t} + \Delta \xi_{l,t}) G_2 x \leqslant G_3 & \forall t, \forall l, \mu_{l,t} \\ \frac{1}{L} \sum\limits_{l=1}^{L} \left| \Delta \xi_{l,t} \right| \leqslant \varepsilon & \forall t, \chi_t \end{cases} \tag{53}$$

where F is the price coefficients matrix of the objective function; x is the planning and operational variables to be decided; J_1 and G_1 are the first coefficient matrices of the equality and inequality constraints, which are multiplied by the decision variable x and do not contain the uncertainty variables of DG and load; J_2 and G_2 are the second coefficient matrices of the equality and inequality constraints, which are multiplied by the decision variable x and contain the uncertainty variables of DG and load; J_3 and G_3 are the constant term matrices for the equality and inequality constraints; $\pi_{l,t}$, $\mu_{l,t}$ and χ_t are the Lagrange duality multipliers for the equality constraints, inequality constraints and the Wasserstein constraints.

The constraints related to uncertainty variables in this model include Wasserstein constraints, DG and load actual energy output/usage constraints, power balance constraints, wind and light abandonment constraints, and demand response constraints. Other constraints are not considered in duality. Constraints containing uncertainty variables are organized as Equation (53).

The max-type function, which represents the worst scenario, is converted into a min-type function using the Lagrange duality method and merged with the outer min-type function. The model is transformed into the following form:

$$\begin{aligned} \min_{x, \pi_{l,t}, \mu_{l,t}, \chi_t} C = \sum_{l=1}^{L} \sum_{t=1}^{T} & \left[\pi_{l,t} J_1 + \pi_{l,t} \hat{\xi}_{l,t} J_2 + \mu_{l,t} G_1 + \mu_{l,t} \hat{\xi}_{l,t} G_2 \right] x \\ & + Fx - \sum_{l=1}^{L} \sum_{t=1}^{T} \left(\pi_{l,t} J_3 + \mu_{l,t} G_3 \right) - \sum_{t=1}^{T} \chi_t \varepsilon \end{aligned} \tag{54}$$

$$\text{s.t.}\begin{cases} \mu_{l,t} \geq 0 \ \forall t, \forall l \\ \chi_t \geq 0 \ \forall t \\ \chi_t \geq L(\pi_{l,t} J_2 + \mu_{l,t} G_2) x \ \forall t, \forall l \end{cases} \tag{55}$$

4.2.3. Transformation of Nonlinear Terms Based on McCormick Relaxation Method

However, the duality transformed model contains bilinear terms $\pi_{l,t}x$ and $\mu_{l,t}x$, it cannot be solved directly. In this paper, McCormick relaxation method is utilized to rewrite it into a linear model [30], and the transformation equation of McCormick relaxation method is as follows:

$$\begin{aligned} & w = zy \\ & z_{\min} \leqslant z \leqslant z_{\max} \\ & y_{\min} \leqslant y \leqslant y_{\max} \\ & w \leqslant z y_{\max} + z_{\min} y - z_{\min} y_{\max} \\ & w \leqslant z_{\max} y + z y_{\min} - z_{\max} y_{\min} \\ & w \geqslant z_{\max} y + z y_{\max} - z_{\max} y_{\max} \\ & w \geqslant z_{\min} y + z y_{\min} - z_{\min} y_{\min} \end{aligned} \tag{56}$$

Equation (56) introduces a new variable w to replace the original bilinear term zy, with constraints to define the range of w. So far, the distributionally robust model has been rewritten as a MISOCP model that can be solved using the solver.

5. Examples

5.1. Overview of the Algorithm

The computer processor utilized for the arithmetic tests in this paper is i5-13600KF, operating at 3.50 GHz with 32.0 GB of RAM. The proposed method was implemented using the YALMIP optimization toolbox within MATLAB R2019a, and solved using IBM ILOG CPLEX 12.8.0.

In order to verify the feasibility of the proposed expansion planning method, this paper employs the Portugal 54 nodes system for analysis, with the topology shown in Figure 3, which contains four substations and 54 source-load nodes. In the figure, blue nodes represent new source-load nodes, solid lines denote existing lines, dotted lines indicate candidate locations for to-be-built lines, and red lines mark the potential installation sites for SOPs and interconnection switches. The project period for this example is set at 20 years, with a discount rate of 0.03. The unit price for demand response incentives is 0.3 CNY/kW, the maximum contract signing ratio is 50%, the price of purchasing power from the superior grid is 0.5 CNY/kW, and the price of selling power to the customers is 0.7 CNY/kW. Parameters of nodes and lines are described in detail in Ref. [31]. In addition, this paper utilizes three-year historical data of DG and various types of loads in a park in Zhongshan City in China's Guangdong Province to construct reference distributions for their temporal characteristics, and the data sampling accuracy is 15min. The relevant parameter settings for devices are shown below.

(1) Line

The construction cost of the line is 150,000 CNY/km, the capacity is 7.27 MW, the length is the straight-line distance between the two nodes, and the line resistance and reactance per unit length are 0.307 Ω/km and 0.38 Ω/km.

(2) SOP

The unit installation capacity is 10 kW, the investment cost is 1000 CNY/kW, the loss coefficient is 0.02, the annual operation and maintenance cost coefficient is 0.01, and the maximum SOP installation capacity of each line is 1 MW.

(3) Interconnection switch

The investment cost for per unit is CNY 100,000, and the annual operation and maintenance cost coefficient is 0.05.

(4) DG

The penalty cost for abandoned wind and solar power is 0.15 CNY/kW, and the maximum reduction ratio is 0.5. The integrated situation is shown in Table 1.

(5) ESS

The annual operation and maintenance cost is 0.35 CNY/kW, the charging and discharging efficiency coefficients are both 0.86, the battery loss coefficient is 0.1, and the maximum and minimum power storage states are 1 and 0.2. The integrated situation is shown in Table 2.

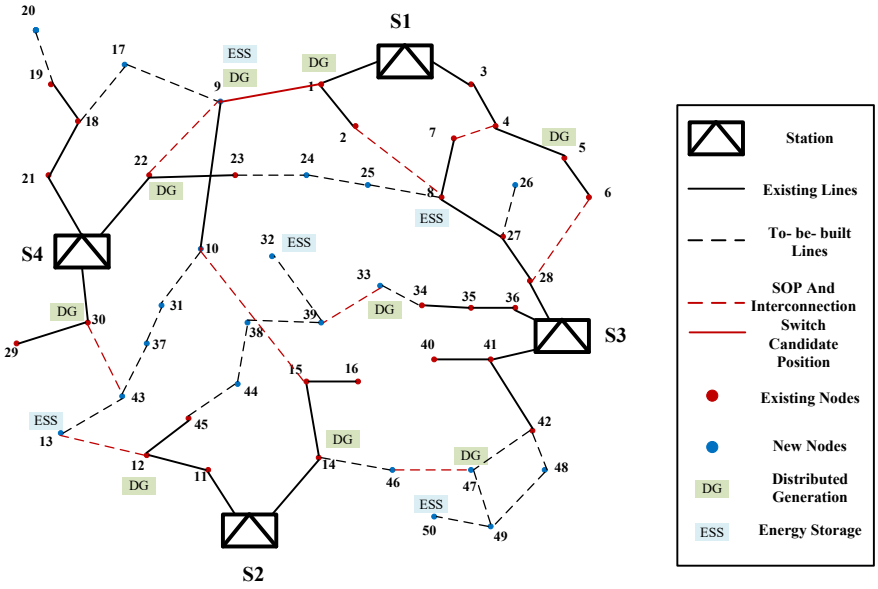

Figure 3. Portugal 54 nodes system topology.

Table 1. Integrated situation of DGs.

Access Node	Maximum Power (kW)	Access Node	Maximum Power (kW)	Access Node	Maximum Power (kW)
1	3900	12	4100	30	3800
5	3500	14	2800	33	4100
9	3600	22	3500	47	4000

Table 2. Integrated situation of ESS.

Access Node	Rated Capacity (kW·h)	Maximum Charging Power (kW)	Maximum Discharge Power (kW)
8	1500	500	500
9	1100	400	400
13	1000	400	400
32	800	300	300
50	900	300	300

5.2. Planning Results and Analysis

In this paper, three planning cases are set up, and their planning results are shown in comparison.

Case 1: Lines expansion planning considering SOPs and interconnection switches;

Case 2: Lines expansion planning considering only SOPs;

Case 3: Lines expansion planning considering only interconnection switches.

After the optimization calculation, the network structures of the three planning schemes are shown in Figures 4–6, the corresponding planning results are shown in Table 3, and the specific costs are shown in Table 4.

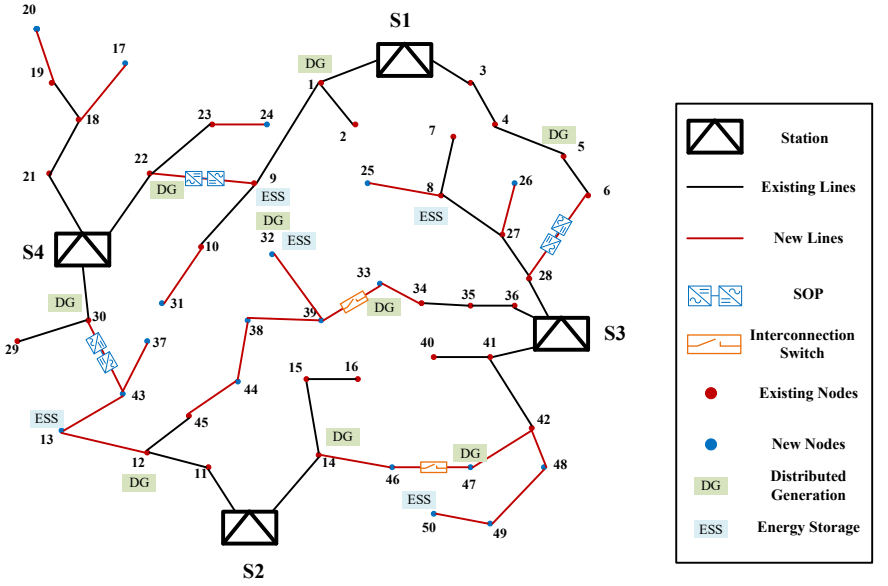

Figure 4. Planning Case 1 network structure.

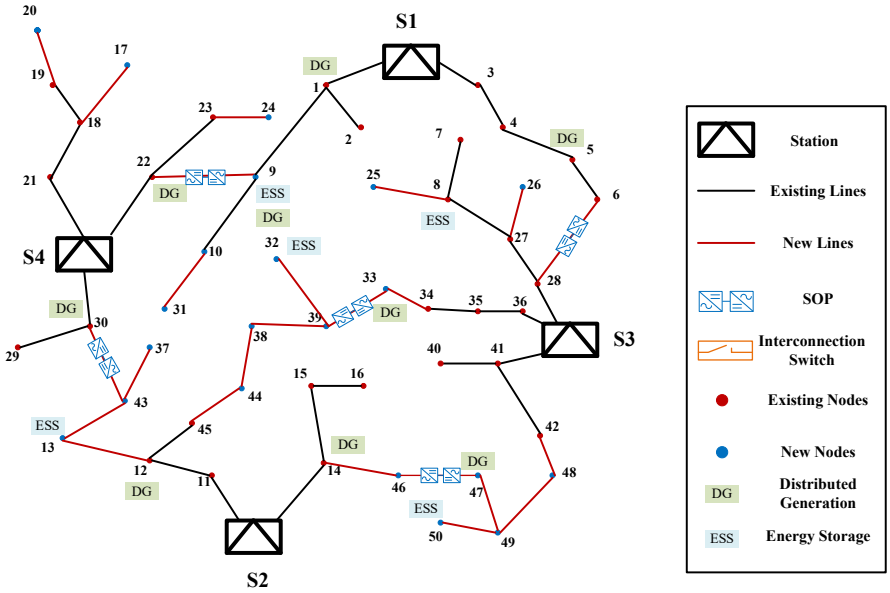

Figure 5. Planning Case 2 network structure.

Table 3. Corresponding planning results of the three cases.

	Case 1	Case 2	Case 3
SOP Planning Location and Capacity (kW)	6–28 (530) 9–22 (610) 30–43 (2150)	6–28 (530) 9–22 (610) 30–43 (2150) 33–39 (450) 46–47 (390)	--
Interconnection Switch Planning Location	33–39 46–47	--	6–28 9–22 12–13 46–47

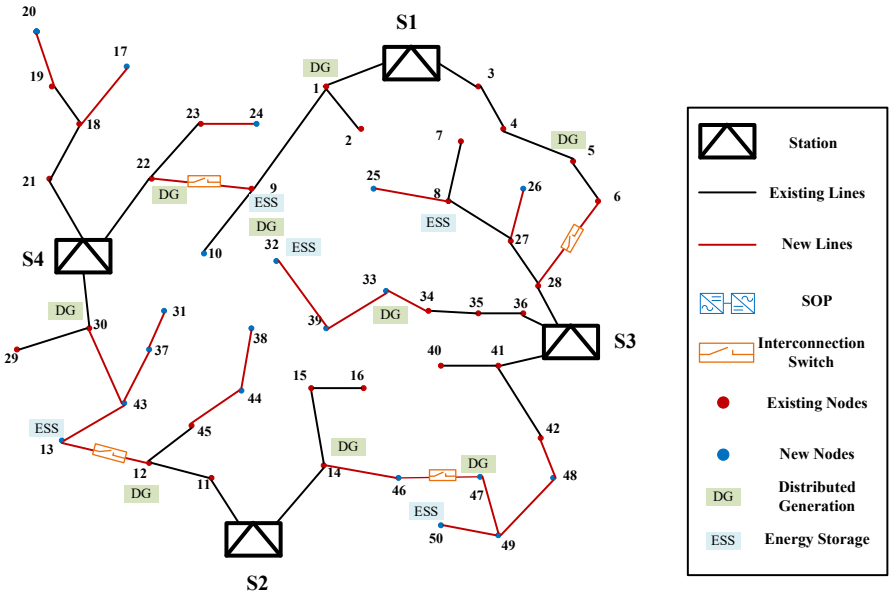

Figure 6. Planning Case 3 network structure.

Table 4. Specific costs of the three cases.

Annual Cost (CNY 10^4)	Case 1	Case 2	Case 3
Lines Equivalent Annual Investment Cost	146.14	146.13	165.23
SOP Equivalent Annual Investment Cost	22.11	27.76	0.00
Interconnection Switches Equivalent Annual Investment Cost	1.34	0.00	2.69
SOP Operation and Maintenance Costs	0.22	0.28	0.00
Interconnection Switches Action Costs	0.07	0.00	0.13
ESS Operation and Maintenance Costs	129.38	131.23	125.56
DR Costs	324.47	323.15	345.25
Wind and Solar Power Penalty Costs	2.51	0.00	18.06
Network and SOP Loss Costs	418.43	417.74	493.87
Revenue from the Purchase and Sale of Electricity	5972.86	5973.29	5839.94
Net Profit of One Year	4928.18	4927.00	4689.15

A comparative analysis of the three cases presented in Table 4 reveals the following conclusions:

(1) Case 2 has the highest annual investment cost and the highest operational profits. Case 3 has the lowest annual investment cost and the lowest operational benefits. Overall, Case 1 has the highest annual net benefit. Compared to that of Case 3, Case 1 has a profit improvement of more than 5%. (2) The DG consumption of Case 1 and Case 2 are better than Case 3. Compared with Case 3, Case 1 and Case 2 increase the annual revenue of purchased and sold electricity and decrease the costs of loss. This demonstrates the role of the SOP in operation. SOPs can adjust the operation and control strategy in real time for each time period, with flexible regulation and control characteristics. (3) The annual investment cost of Case 2 is 2.5% higher than Case 1, yet its operation benefit is only 0.6% higher than Case 1, demonstrating the economic advantage of the interconnection switches.

5.3. Impact of SOPs on Distribution Network Operation

All SOPs in Case 1 were replaced with interconnection switches to obtain Case 4, and the planning scheme of Case 4 was simulated. Assuming that the maximum DG curtailment rate is 1, the optimal operation costs of the two cases are shown in Table 5. The impact of SOPs on operation was further analyzed, and the two cases were evaluated and compared in terms of three indicators, including network and SOP loss, DG accommodation rate, and average line loading rate, and the results are shown in Figure 7.

Table 5. Comparison of the optimal operation costs of case1 and case 4.

Annual Cost (CNY 10^4)	Option 1	Option 4
SOP Operation and Maintenance Costs	0.22	0
Interconnection Switches Action Costs	0.07	0.175
ESS Operation and Maintenance Costs	129.38	124.86
Demand Response Costs	324.47	343.81
Wind and Solar Power Penalty Costs	2.51	19.37
Net Loss and SOP Loss Costs	418.43	501.35
Revenue from the Purchase and Sale of Electricity	5972.86	5796.72
Annual Operating Income	5097.78	4807.155

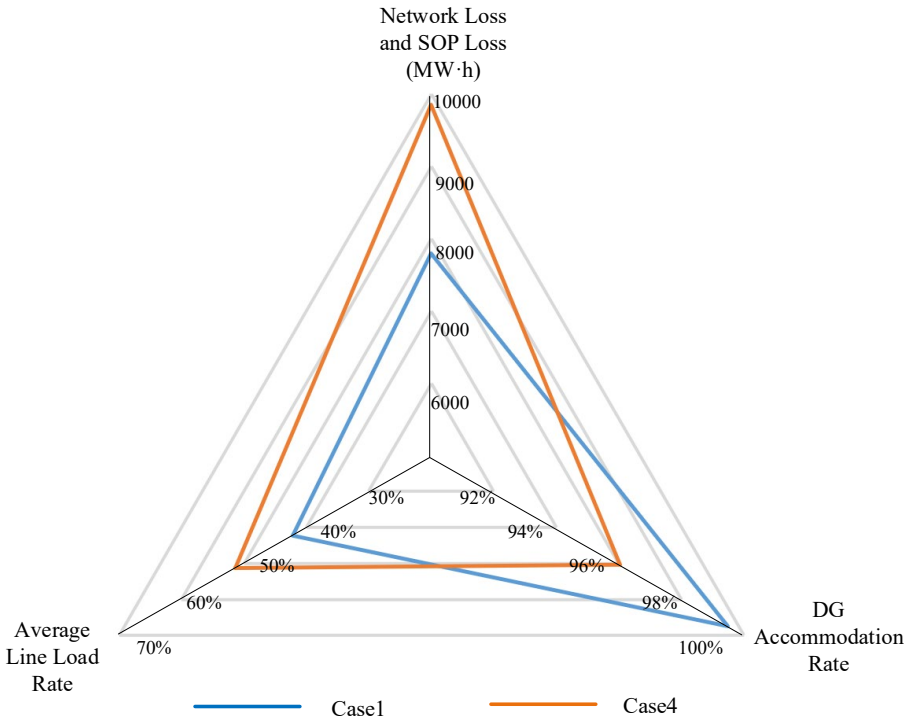

Figure 7. Comparison of the operation indexes of Case 1 and Case 4.

From Table 5, it can be seen that Case 4 has lower operation profit, which is reduced by more than 6% compared to Case 1. From Figure 7, Case 1 has less network loss and SOP loss. The application of SOPs makes the network power distribution of Case 1 better than Case 4. Compared with Case 4, the average line load rate in Case 1 increases from 42.19% to 51.36%, which is because the SOPs in Case 1 improve the power flow distribution and load distribution of branches, and enhance the line power supply capacity. From the perspective of low-carbon, Case 1 basically realizes the complete consumption of new energy, while that of Case 4 is only 96.05%, which is due to the fact that an SOP can flexibly regulate the DG injected power among lines, thus it can better realize the consumption of DG and reduce the carbon emission.

5.4. Impact of SOP and Interconnection Switch Cost on Planning Result

Although the flexible regulating ability of an SOP has an advantage over the rigid regulating ability of an interconnection switch, the high investment cost of an SOP leads to its limited use. In order to study the impact of SOP and interconnection switch investment cost on planning result, 10 cases are designed here, in which the unit capacity investment cost of an SOP gradually decreases from 1000 CNY/kW to 100 CNY/kW in steps of CNY 100, the investment cost of one interconnection switch is CNY 100,000, and the rest of the parameters remain unchanged. This case setup allows the SOP cost to gradually equal

or even outperform interconnection switches in the middle and late stages of investment. The planning schemes are shown in Figure 8.

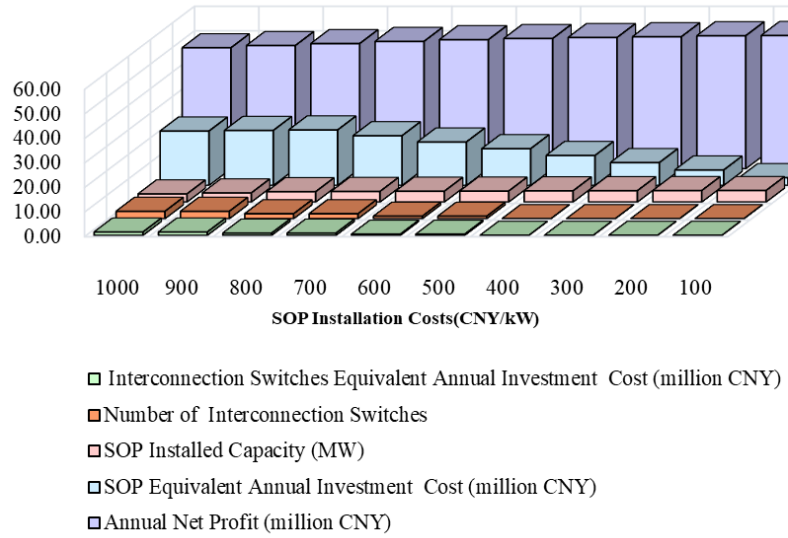

Figure 8. Impact of sop and interconnection switch costs on planning results.

As can be seen from Figure 8, the SOP installed capacity gradually increases as the investment cost of per unit capacity decreases, and the capacity no longer changes after a certain level. The number of interconnection switches gradually decreases. This is due to the fact that in the early stage of SOP development, its installed capacity is limited by the investment cost. As the development of the SOP, the interconnection switches are all replaced by SOPs, and the installed capacity of the SOP grows slowly. As the SOP installed capacity increases, the annual net profit gradually increases. This is because the distribution network optimizes the operation status of the ESS and other devices through the SOP, increases the DG accommodation rate and reduces the cost of purchasing power from the main grid.

5.5. Validity Analysis of Distributionally Robust Optimization Method

This paper introduces a distributionally robust collaborative planning method based on the Wasserstein distance. The comparative results with deterministic optimization and robust optimization are presented in Table 6. Deterministic optimization here refers to stochastic optimization based on multiple scenarios.

Table 6. Comparison of results of different methods.

Annual Cost (CNY 10^4)	Deterministic Optimization	Robust Optimization	Distributionally Robust Optimization
Lines Equivalent Annual Investment Cost	146.14	146.14	146.14
SOP Equivalent Annual Investment Cost	16.11	30.48	22.11
Interconnection Switches Equivalent Annual Investment Cost	1.34	1.34	1.34
SOP Operation and Maintenance Costs	0.16	0.30	0.22
Interconnection Switches Action Costs	0.07	0.07	0.07
ESS Operation and Maintenance Costs	123.83	138.49	129.38
DR Costs	291.35	342.75	324.47
Wind and Solar Power Penalty Costs	0	5.28	2.51
Network and SOP Loss Costs	391.37	449.43	418.43
Revenue from the Purchase and Sale of Electricity	6059.86	5884.29	5972.86
Net Profit of One Year	5089.49	4770.01	4928.18

As shown in Table 6, the deterministic optimization method has the highest annual net profit. However, it is too ideal to ensure the reliability of system operation. The robust optimization method is more conservative and ensures the reliability of system operation, but has the least profit. The distributionally robust optimization method properly portrays the worst scenario, and its annual net profit is between the other two methods, which not only overcomes the conservation of the robust optimization, but also ensures the reliability of the system operation. Compared with the traditional robust method, its annual net profit is improved by more than 3%.

5.6. Validity Analysis of the McCormick Relaxation Method

Compared with the original bilinear model, the use of McCormick relaxation method inevitably introduces some approximation in the computation of bilinear terms $\pi_{l,t}x$ and $\mu_{l,t}x$. The power injection of SOPs at each moment is selected, and the maximum relative error of the power injection of SOPs is calculated at all nodes separately, and the calculation equation is shown below:

$$\eta_{\text{error}} = \max_{i \in \Psi_{node}} \left\{ \frac{\left| P_{i,t}^{\text{SOP}} - P_{i,t}^{\text{SOP,ref}} \right|}{P_{i,t}^{\text{SOP,ref}}} \times 100\% \right\} \tag{57}$$

where $P_{i,t}^{\text{SOP,ref}}$ is the reference value obtained by using the nonlinear equation. Comparing the results processed by McCormick relaxation with the reference values and yields the maximum relative error of SOP power injection in a day as shown in Figure 9.

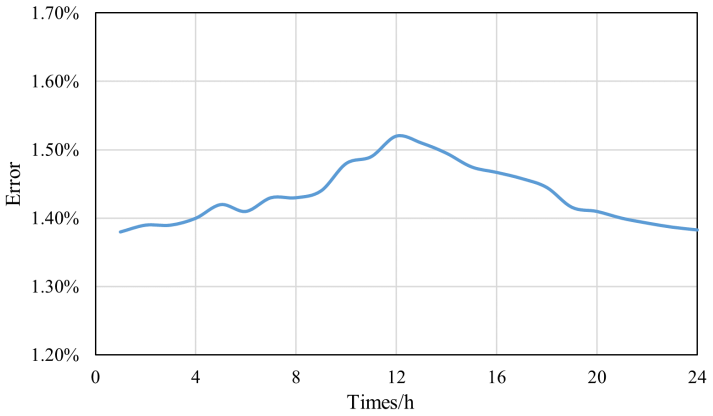

Figure 9. Maximum relative error chart.

As can be seen in Figure 8, the maximum relative error between the calculated value and the reference value for each time period does not exceed 1.55%, which is within the acceptable error range [32], validating the effectiveness of the McCormick relaxation method.

To verify the superiority of McCormick method in this model, it is compared with IPOPT [33] (Interior Point Optimizer) and the bilinear-removed method [30]. Table 7 demonstrates the performance of the three methods, including the annual net profit and the computing time.

Table 7. Performance comparison of three methods.

	IPOPT	Bilinear-Removed	McCormick
Annual Net Profit (CNY 10^7)	--	3.75	4.93
Computing Time (h)	>5	1.59	2.52

As can be seen in Table 7, the McCormick method computes the most annual net profit for the optimal solution. Due to the large size of the problem and the large number of both continuous and 0–1 variables, IPOPT was unable to obtain an optimal solution within 5 h. Since there is more than one bilinear term in the objective function, although the bilinear-removed method takes the least amount of time, its computational result is only 76% of that of McCormick method. The superiority of the McCormick relaxation method is verified.

6. Conclusions

This paper introduces an expansion planning method capable of achieving the coordinated planning of SOPs, interconnection switches and lines. Compared with the planning schemes considering only interconnection switches or SOPs, the planning scheme obtained by this method had better economy. This method can optimize the system operation and improve the system reliability while improving the economy by nearly 5%.

Considering the uncertainty of the source-load timing characteristics, this paper proposes a distributionally robust collaborative planning model based on the Wasserstein distance, which is an uncertainty handling method. This method guarantees the reliability of the system while improving the economy by more than 3% compared to the traditional robust method. Further, in this paper, the model is solved analytically using various methods such as Lagrange duality and McCormick relaxation method.

There are still some deficiencies in this paper. This paper only considers the installation of a two-port SOP and does not comprehensively consider the provisions of existing planning and design guidelines for feeder connection forms. In the future, with the development of new power electronic technology and flexible distribution network, it is necessary to study multi-port SOPs and more complex expansion planning scenarios, and to seek more accurate and efficient solution algorithms.

Author Contributions: Conceptualization, S.L.; Methodology, M.B. and C.H.; Software, M.B.; Validation, S.L.; Formal analysis, X.W.; Investigation, J.L. and C.H.; Data curation, J.L.; Writing—original draft, M.B.; Writing—review & editing, S.L.; Project administration, J.L. and X.W.; Funding acquisition, C.H. All authors have read and agreed to the published version of the manuscript.

Funding: This research is funded by Science and Technology Project of the China Southern Power Grid Company, grant number: 032000KK52222013(GDKJXM20222118).

Data Availability Statement: Data are contained within the article.

Acknowledgments: The authors would like to express their gratitude to all those who helped them during the writing of this paper. The authors would like to thank the reviewers for their valuable comments and suggestions.

Conflicts of Interest: Authors Jianchu Liu and Changhao He were employed by Zhongshan Power Supply Bureau, Guangdong Power Grid Co., Ltd., Xinghang Weng was employed by Power Grid Planning Center of Guangdong Power Grid Co., Ltd. The authors declare that the research was conducted in the absence of any commercial or financial relationships that could be construed as a potential conflict of interest. The authors declare that this study received funding from Science and Technology Project of the China Southern Power Grid Company. The funder was not involved in the study design, collection, analysis, interpretation of data, the writing of this article or the decision to submit it for publication.

References

1. Jacob, R.A.; Zhang, J. Distribution network reconfiguration to increase photovoltaic hosting capacity. In Proceedings of the 2020 IEEE Power & Energy Society General Meeting (PESGM), Montreal, QC, Canada, 2–6 August 2020.
2. Wang, X.D.; Wu, W.C.; Liu, L.; Liu, H.T.; Pan, D. Multiparameter programming based capacity assessment method of distributed photovoltaic for active distribution network. *Autom. Electr. Power Syst.* **2018**, *42*, 20–26.
3. Wang, C.S.; Ji, J.; Ji, H.R.; Yu, H.; Wu, J.Z.; Li, P. Technologies and Application of Soft Open Points in Distribution Networks. *Autom. Electr. Power Syst.* **2022**, *46*, 1–14.

4. Chen, Y.; Tang, W.; Chen, X.Y.; Cong, P.W.; Zhang, L. Tie switch allocation optimization based on dynamic segment of equivalent load-PV curve. *Electr. Power Autom. Equip.* **2015**, *35*, 47–53.
5. He, Y.; Wu, H.; Bi, R.; Qiu, R.J.; Ding, M.; Sun, M.; Xu, B.; Sun, L. Coordinated planning of distributed generation and soft open points in active distribution network based on complete information dynamic game. *Int. J. Electr. Power Energy Syst.* **2022**, *138*, 107953. [CrossRef]
6. Pamshetti, V.B.; Singh, S.; Thakur, A.K.; Singh, S.P.; Babu, T.S.; Patnaik, N.; Krishna, G.H. Cooperative operational planning model for distributed energy resources with soft open point in active distribution network. *IEEE Trans. Ind. Appl.* **2022**, *59*, 2140–2151. [CrossRef]
7. Zhang, S.X.; Wang, H.R.; Li, R.; Cheng, H.Z.; Fang, Y.C.; Li, K.; Wang, X.; Xiang, Y. Active Distribution Network Expansion Planning Method Considering the Integration of Soft Open Point. *Proc. CSEE* **2023**, *43*, 48–61.
8. Zhang, J.; Foley, A.M.; Wang, S. Optimal planning of a soft open point in a distribution network subject to typhoons. *International J. Electr. Power Energy Syst.* **2021**, *129*, 106839. [CrossRef]
9. Li, P.; Ji, J.; Chen, S.R.; Ji, H.R.; Xu, J.; Song, G.Y.; Zhao, J.L.; Wu, J.Z.; Wang, C.S. Multi-stage expansion planning of energy storage integrated soft open points considering tie-line reconstruction. *Prot. Control. Mod. Power Syst.* **2022**, *7*, 45. [CrossRef]
10. Ehsanbakhsh, M.; Sepasian, M.S. Simultaneous siting and sizing of Soft Open Points and the allocation of tie switches in active distribution network considering network reconfiguration. *IET Gener. Transm. Distrib.* **2023**, *17*, 263–280. [CrossRef]
11. Ehsan, A.; Yang, Q. State-of-the-art techniques for modelling of uncertainties in active distribution network planning: A review. *Appl. Energy* **2019**, *239*, 1509–1523. [CrossRef]
12. Li, Z.M.; Xu, Y.; Feng, X.; Wu, Q.W. Optimal stochastic deployment of heterogeneous energy storage in a residential multienergy microgrid with demand-side management. *IEEE Trans. Ind. Inform.* **2020**, *17*, 991–1004. [CrossRef]
13. Zuo, F.Y.; Zhang, Y.Q.; Zhao, Q. Two-stage Stochastic Optimization for Operation Scheduling and Capacity Allocation of Integrated Energy Production Unit Considering Supply and Demand Uncertainty. *Proc. Chin. Soc. Electr. Eng.* **2022**, *42*, 8205–8215.
14. Ghaemi, S.; Salehi, J. Incorporating ramp problem into the expansion planning of distributed energy resources for improving flexibility of renewable -based distribution network using interval optimization. *Electr. Eng.* **2021**, *103*, 341–355. [CrossRef]
15. Dong, Y.; Zhang, H.; Ma, P.; Wang, C.; Zhou, X.J. A hybrid robust-interval optimization approach for integrated energy systems planning under uncertainties. *Energy* **2023**, *274*, 127267. [CrossRef]
16. Ehsan, A.; Yang, Q.; Cheng, M. A scenario-based robust investment planning model for multi-type distributed generation under uncertainties. *IET Gener. Transm. Distrib.* **2018**, *12*, 4426–4434. [CrossRef]
17. Huang, H.X.; Li, Z.M.; Gooi, H.B.; Qiu, H.F.; Zhang, X.T.; Lu, C.X.; Liang, R.; Gong, D.W. Distributionally robust energy-transportation coordination in coal mine integrated energy systems. *Appl. Energy* **2023**, *333*, 120577. [CrossRef]
18. Jiang, Y.P.; Ren, Z.Y.; Li, W.Y. Committed Carbon Emission Operation Region for Integrated Energy Systems: Concepts and Analyses. *IEEE Trans. Sustain. Energy* **2023**, *15*, 1194–1209. [CrossRef]
19. Ge, S.Y.; Du, Y.M.; Guo, Y.; Cui, K.; Liu, H.; Li, J.K. Day-ahead Energy Management and Trading of Electric Vehicle, Charging Station and Distribution Network Based on Distributionally Robust Optimization. *Autom. Electr. Power Syst.* **2024**, *48*, 11–20.
20. Ge, S.Y.; Fan, Q.F.; Liu, H.; Han, J.; Cheng, L.; Xu, Z.Y.; Cai, C. Distributionally Robust Optimization Method for Substation Planning Considering Incentive-based Response Uncertainty. *Autom. Electr. Power Syst.* **2023**, *47*, 80–89.
21. Zhu, R.J.; Wei, H.; Bai, X.Q. Wasserstein metric based distributionally robust approximate framework for unit commitment. *IEEE Trans. Power Syst.* **2019**, *34*, 2991–3001. [CrossRef]
22. Wang, S.; Luo, F.; Dong, Z.Y.; Ranzi, G. Joint planning of active distribution networks considering renewable power uncertainty. *Int. J. Electr. Power Energy Syst.* **2019**, *110*, 696–704. [CrossRef]
23. De Barros, H.F.; Alvarez-Herault, M.C.; Raison, B.; Tran, Q.T. Optimal AC/DC Distribution Systems Expansion Planning from DSO's Perspective Considering Topological Constraints. *IEEE Trans. Power Deliv.* **2023**, *38*, 3417–3428. [CrossRef]
24. Wang, C.S.; Song, G.Y.; Li, P.; Ji, H.R.; Zhao, J.L.; Wu, J.Z. Optimal Configuration of Soft Open Point for Active Distribution Network Considering the Characteristics of Distributed Generation. *Engineering* **2017**, *37*, 1889–1897.
25. Li, J.K.; Ge, S.Y.; Liu, H.; Zhang, S.D.; Wang, C.S.; Wang, P.X. Distribution locational pricing mechanisms for flexible interconnected distribution system with variable renewable energy generation. *Appl. Energy* **2023**, *335*, 120476. [CrossRef]
26. Wang, C.; Gao, R.; Wei, W.; Shafie-khah, M.; Bi, T.S.; Catalão, J. Risk-based distributionally robust optimal gas-power flow with Wasserstein distance. *IEEE Trans. Power Syst.* **2019**, *34*, 2190–2204. [CrossRef]
27. Song, G.Y. Operation and Planning Method of Soft Open Point for Multiple Scenarios in Active Distribution Network. Ph.D. Thesis, Tianjin University, Tianjin, China, 2017.
28. Lin, Z.; Hu, Z.C.; Song, Y.H. Convex Relaxation for Optimal Power Flow Problem: A Recent Review. *Proc. CSEE* **2019**, *39*, 3717–3728.
29. Esfahani, P.M.; Kuhn, D. Data-driven distributionally robust optimization using the Wasserstein metric: Performance guarantees and tractable reformulations. *Math. Program.* **2018**, *171*, 115–166. [CrossRef]
30. Deng, L.R.; Sun, H.B.; Li, B.J.; Sun, Y.; Yang, T.S.; Zhang, X. Optimal operation of integrated heat and electricity systems: A tightening McCormick approach. *Engineering* **2021**, *7*, 1076–1086. [CrossRef]
31. Miranda, V.; Ranito, J.; Proenca, L. Genetic algorithms in optimal multistage distribution network planning. *IEEE Trans. Power Syst.* **1994**, *9*, 1927–1933. [CrossRef]

32. Xu, X.S.; Xu, C.R.; Li, M.S.; Ji, T.Y. Optimization Dispatching Model of the Combined Heat and Power System Considering Wind Power Optimization Dispatching Model of the Combined Heat and Power System Considering Wind Power Consumption. *South. Power Syst. Technol.* **2024**, *in press*.
33. Yang, C.; Li, Z.S. Conditional Distributionally Robust Optimization of Integrated Electricity and Heat Systems with Variable Flow Regulation Modes. *Proc. CSEE* **2024**, *in press*.